Analysis of Nano-hardness Distribution Near the Ferrite-martensite Interface in a Dual Phase Steel with Factorization of Its Scattering Behavior

Reon ANDO,[1] Takashi MATSUNO,[1]* Tomoko MATSUDA,[2] Norio YAMASHITA[3] Hideo YOKOTA,[3] Kenta GOTO[4] and Ikumu WATANABE[4]

1) Tottori University, 4-101 Koyama-cho-minami, Tottori-City, Tottori, 680-8552 Japan.
2) Tottori Institute of Industrial Technology, 1247 Kusaka, Yonago-City, Tottori, 689-3522 Japan.
3) Riken Center for Advanced Photonics, Riken, 2-1 Hirosawa, Wako, Saitama, 351-0198 Japan.
4) Research Center for Structural Materials, National Institute for Materials Science, 1-2-1 Sengen, Tsukuba, Ibaraki, 305-0047 Japan.

Herein, we investigated the local preliminary hardening of ferrite near the ferrite–martensite interfaces in a dual-phase (DP) steel. Geometrically necessary dislocations (GNDs), generated due to interfacial misfit between different phases, may cause preliminary hardening of ferrite around such interfaces. However, for nano-hardness distribution, the hardened zone was not evidently detected by scattering measurement. Thus, we factorized nano-hardness scattering to estimate the actual ferrite hardness near ferrite–martensite interfaces.

First, nano-hardness was measured around a martensite island using a conical nano-indenter in the DP steel containing 10% martensite by volume. Taking into account the scattering, the nano-hardness measurement converged to the hardness of ferrite, exceeding the distance corresponding to the nano-indenter radius. Thus, a preliminary hardening zone was not detected. Subsequently, the surface of the nano-indented microstructure was polished and observed using scanning electron microscopy (SEM) by analyzing electron back scattering diffraction (EBSD). This analysis confirmed the presence of the nano-indented microstructure under ferrite. Moreover, it established that the majority of the irregularly higher nano-hardness was caused by the buried martensite under ferrite. The value of the kernel average misorientation (KAM), which is proportional to the GND density for other irregularly higher nano-hardness points, was higher for the nano-indented microstructure as compared to that of the buried martensite. On the other hand, the ferrite was expanded under the nano-indented points for the majority of the irregularly lower nano-hardness, with some exceptions. Further, soft martensite was observed to induce irregularly lower nano-hardness locally around the interface.

KEY WORDS: dual phase steel; grains and interfaces; scattering; nanoindentation; serial sectioning.

1. Introduction

Dual-phase (DP) steel, composed of hard martensite and soft ferrite, has been widely used in automotive applications owing to its superior formability and crashworthiness.[1–3] Although the use of ultra-high-strength steel sheets with a tensile strength of up to 1 310 MPa grade is increasing, there is still a substantial industrial demand for steel sheets with high strength and ductility. Therefore, extensive research on DP steel has been conducted for improving its strength and ductility. Thus far, the volume fraction, morphology, and hardness of martensite islands and their effects on the mechanical properties of DP steel have been established. Hasegawa et al.[4] reported that the plastic strain of martensite in tensile deformation increases proportionally with martensite volume fraction, thereby increasing the tensile strength.[5] Kurita et al.[6] reported that the fatigue fracture of DP steel strongly correlates with martensite deformation. Several other researchers have reported that the grain size, shape, and spatial distribution of martensite determine the strength and ductility of DP steels.[7–11]

In addition to the morphological effects on the strength and ductility of DP steel, recent research has been focused on the mechanical properties near the ferrite–martensite

* Corresponding author: E-mail: matsu@tottori-u.ac.jp

interface. Kadkhodapour *et al.*[12] reported the existence of a local hardening site that increased the strength of DP steels. The presence of this site was established via microscale finite element (FE) simulations, and the researchers suggested that this local hardening site was formed by geometrically necessary dislocations (GNDs) around the ferrite–martensite interface, wherein the GNDs pinned the movable dislocations to increase the flow stress. To distinguish this local hardening from the material deformation, hereafter we call it as "preliminary hardening site." Ramazani *et al.*[13] detailed the formation mechanism of this preliminary hardening site to confirm its existence.

As mentioned above, the preliminary hardening site was reported to contribute to the strengthening of DP steels. However, this contribution is limited to fine-grained DP steels. Consequently, the effect of the preliminary hardening site remains undetermined in conventional DP steel with coarse grains. Conversely, with respect to ductile fractures, it should be considered that microvoid formation is often initiated from the ferrite–martensite interface.[14–16] Therefore, the local hardness near the interface may play an important role in the ductile fracture of conventional DP steels with coarse grains. The role of the local hardness around the ferrite–martensite interface in the ductile fractures must be determined for conventional DP steels.

With the above-mentioned background, our previous research focused on the nano-hardness distribution of ferrites near the ferrite–martensite interface in coarse-grained DP steel. We found that the FE simulation of nanoindentation without the preliminary hardening site produced consistent results with the actual nano-hardness distribution around the ferrite–martensite interface.[17] Put differently, the preliminary hardening site was found to be absent in our previous study. However, we should consider that the nano-hardness involved a large degree of scattering. Kadkhodapour *et al.*[12] also measured the nano-hardness scattering around the interface, although the detailed mechanism was not discussed. Furthermore, it has been opined that the martensite islands under the indented ferrite surface could have caused this scattering.[18] Notably, the actual martensite has a complicated three-dimensional shape, indicating that different phases are hidden under the nanoindentations. Such hidden phases were undetected in the previous studies; herein, we regarded the nano-hardness scattering as noise caused by the hidden martensite, based on previous reports.

The nano-hardness scattering could have been caused by the spotty distribution of preliminary hardening sites. Therefore, the factors influencing the nano-hardness scattering around the ferrite–martensite interface are classified in this study. To expose the hidden shape of the ferrite–martensite interface under the nanoindentation, the 2.5-μm thickness layer on the indented surface was sheared off by polishing. Thereafter, the irregularly high or low nano-hardness was classified depending on whether it was caused by the hidden interface shape. The preliminary local hardening sites can be found in the form of inconsistent hardening (or softening) sites with the hidden interface shape. Scanning electron microscopy (SEM) and electron back scattering diffraction (EBSD) were used for microstructural identification. Furthermore, the preliminary hardening sites, which were directly related to GND density, were analyzed using EBSD misorientation measurements.

2. Experimental Conditions

2.1. Material

The chemical composition of the sample used in this study is listed in **Table 1**. The ingot, which was created by vacuum melting, was thinned to a 6.0 mm-thick sheet by hot rolling at 1 173 K. After the sheet was cooled to 923 K in air, it was water-quenched to room temperature (300 K).

Figure 1 shows the optical micrograph of the DP steel after LePera etching,[19] wherein the dark- and white-colored grains represent ferrite and martensite, respectively. This DP steel contained a volume fraction of approximately 10% martensite, which was evaluated by the image analysis of the area fraction. The average grain sizes of the ferrite and martensite were 11.5 and 7.1 μm, respectively, as calculated using the linear intercept method. The microhardness values, as measured via conical nanoindentation with an indent force of 10 000 μN, were found to be 2.1 and 8.7 GPa for the martensite and ferrite, respectively. Both values were averages of measurements at three points.

The mechanical properties of the DP steel are shown in **Table 2**. Although the tensile strength was slightly lower than the standardized value, the mechanical properties were similar to those of 590 MPa grade steel.

2.2. Nanoindentation

The nano-hardness of ferrite around the ferrite–martensite

Table 1. Chemical compositions of the DP steel (mass%).

C	Si	Mn	S	Al	N
0.049	0.49	1.99	0.0013	0.029	0.0007

Table 2. Mechanical properties of the DP steel.

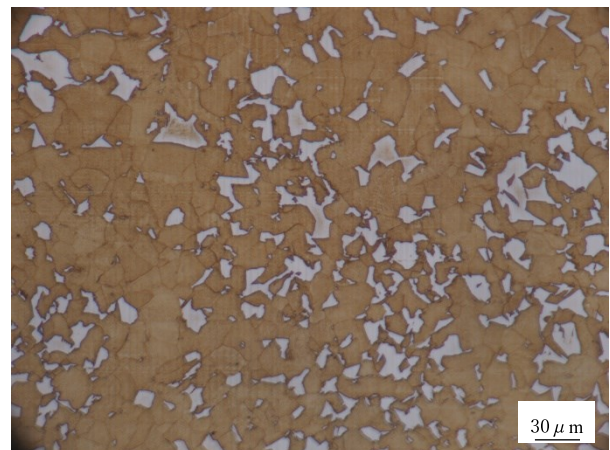| Yield stress [MPa]	Tensile strength [MPa]	Uniform elongation [%]	Total elongation [%]
288	574	17.9	32.8

Fig. 1. Optical micrograph of the LePera-etched DP steel. White grains are martensite, while the others are ferrite. (Online version in color.)

interface was measured using the Hysitron TI 950 TriboIndenter (Bruker), whereby the indentation was performed with forces of 1 000 and 2 000 μN. A conical indenter with a vertical angle of 90° was used to avoid the non-uniqueness in evaluating the distance to the interface. For the case with the Bercovich indenter, the actual distances between the interface and a nano-indent were expected to be diverse among some indents owing to the non-axisymmetric indenter shape. The length between the indent center and the closest part of the ferrite–martensite interface was evaluated as a distance, as shown in **Fig. 2**.

Based on nanoindentation, the unevenness of the material surface was regarded as a unique factor. The differences between the heights of the two phases resulted in the deviation in the nano-hardness measurements from the true values. Therefore, we paid special attention to polishing the material surface for the nanoindentation measurements. Firstly, the material was polished with a 4 000-grit waterproof paper. Thereafter, the surface was further polished with 1 μm-granite particle polishers. Colloidal silica was used to finali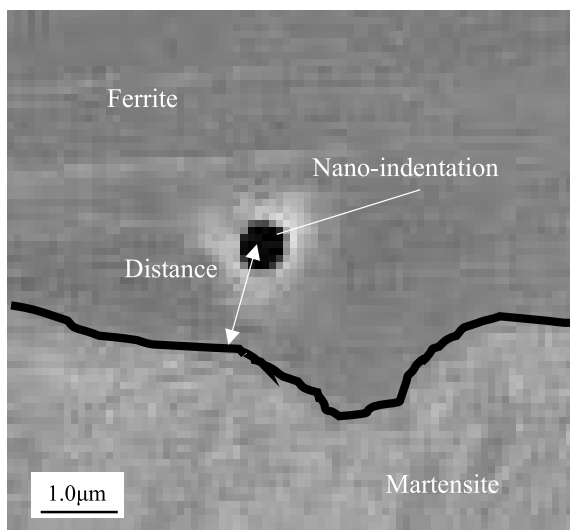ze the polishing, and a nanoscale flat surface was eventually achieved. **Figure 3** shows the height contour of the polished surface with nanoindentation, whereby the height was measured via scanning probe microscopy. This figure suggests that the height of the ferrite and martensite surfaces are similar around their interface.

Regarding the sites for nano-hardness evaluation, nanoindentation measurements were performed at the sites within the distance of 0.0–2.0 μm from the ferrite–martensite interface. To avoid mutual interference among the neighboring indents, each nanoindentation was performed such that the indent centers were at a distance of at least five times the indent size.

We defined the three areas, α, β, and γ, where nanoindentations were performed around one martensite island for the area α, around one ferrite grain (including multiple martensite islands) for area β, and one martensite island for area γ. Each area included 6–9 nano-indents. The indentation force for areas α and β was set to 1 000 μN, while that for area γ was set to 2 000 μN. The two variations in the indentation forces were used to determine the influence of the indentation force on nano-hardness.

2.3. Analyzing the Microstructure Around Indents

The proposed study aims to investigate the nano-hardness scattering around the ferrite–martensite interface connected to the hidden microstructure under the indented surface. To achieve this, the material surface, on which the nanoindentation measurements were performed, was slightly polished to observe the initially hidden microstructure.

For microstructural characterization, Hitachi High-Tech Corporation SEM (SU5000) combined with Ametek EBSD were used. The EBSD step size was set to 0.04 μm. In addition to the microstructural appearance obtained from the SEM images, EBSD provided information on the crystal orientation as the inverse pole figure (IPF). Aside from these values, the image quality (IQ) was also obtained via EBSD to classify the ferrite and martensite more accurately. Furthermore, the kernel average misorientation (KAM) values were evaluated to analyze the GND density distribution, whereby the KAM values were calculated by averaging the differences in the crystal orientations at neighboring points in the EBSD measurements; GND density was approximately proportional to the KAM values.[20]

From the viewpoint of polishing the nano-indented surface, microscale thin layers were removed in two steps. Herein, 0.05-μm-alumina was used for this polishing. Moreover, the cross-section polisher was used to obtain clear EBSD maps. As a result of these polishing processes, microstructures with depths of 2.50 and 4.86 μm from the initial surface were exposed and observed.

The thickness dimensions of the above-mentioned sheared-off layers were evaluated using the change in the size of the Vickers indents with an indentation force of 0.02 N. **Figure 4** shows a schematic of the relationship between polished thickness and Vickers indent size. In Fig. 4, d_1 and d_2 represent the lengths of the diagonal of the Vickers indent before and after polishing, respectively. The polishing depth, h, was calculated using the following equation:

Fig. 2. Distance definition between nanoindentation and ferrite-martensite interface in the DP steel.
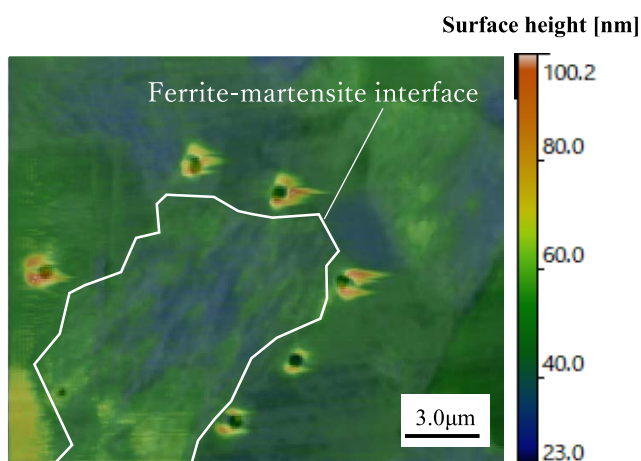

Fig. 3. Surface height map overlaid on the SEM image around a martensite grain, where nanoindentation was conducted near the interface. (Online version in color.)

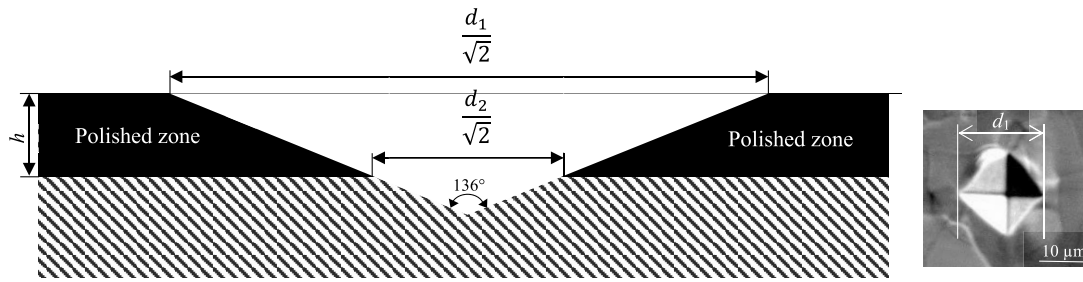$$h = \frac{d_1 - d_2}{2\sqrt{2}\sin 68°}. \quad\quad\quad\quad (1)$$

Fig. 4. Schematic image for evaluation method of the polishing depth by measuring Vickers indentation size.
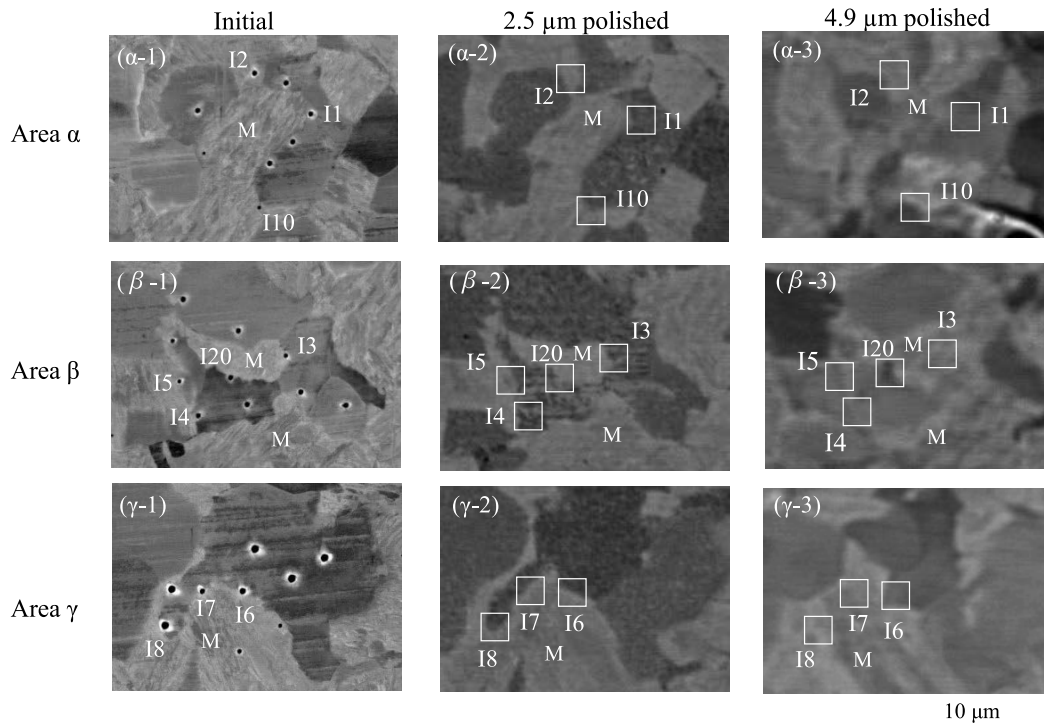

Fig. 5. SEM images of microstructures around the nanoindentations before and after polish. The symbol M denotes the martensite islands.

3. Results

3.1. SEM Observations

Figure 5 shows the SEM images of the nano-indents and their surrounding microstructures. The initially hidden microstructures, which were exposed by polishing, are also shown in Fig. 5. To discuss the nano-hardness scattering, the identifiers I1–I8 were used for some indents that demonstrated nano-hardness scattering. The scattering was defined as the deviated values from the exponential decrease curve of the nano-hardness versus the distance from the interface. From our previous report, the nano-hardness of the ferrite exponentially decreases with an increase in the distance.[17]

As shown in Figs. 5(α-1), 5(β-1), and 5(γ-1), nanoindentation was successfully performed very close to the ferrite–martensite interface. Although the ferrite and martensite were identifiable from the SEM images, the different phases were more accurately observed from the IPF and IQ maps obtained via EBSD. Subsequently, the discussion on the ferrite and martensite shapes exposed by polishing is provided in Section 3.2.

Conversely, the SEM images provided clearer indent shapes than as obtained in the EBSD analysis. The average diameter of the nanoindentations in areas α and β (at an indentation force of 1 000 μN) was 0.569 μm, whereas that in area γ (indentation force of 2 000 μN) was 1.17 μm.

3.2. EBSD Analysis

Figure 6 shows the IQ maps overlaid on the IPF maps obtained via EBSD. The areas shown in Fig. 6 are the same as those in the SEM images in Fig. 5. The ferrite and martensite in Fig. 5 are more easily distinguishable in Fig. 6. From Figs. 6(α-1)–6(α-3), the shrinkage/disappearance of martensite was observed at the polished surface under indent I1 in area α. Conversely, hidden martensite appeared at the polished ferrite surface around indent I2. Figs. 6(β-1)–6(β-3) show that the interface shape around indents I3 and I4 in area β was maintained after two polishing processes. Similar to indent I2, the martensite appeared at the polished ferrite surface around indent I5. For the remaining indents in area γ (as shown in Figs. 6(γ-1)–6(γ-3)), the interface shape hidden under indent I6 was similar to that on the initial surface. As in the cases of indents I2 and I5, martensite also appeared at the polished ferrite surface around indents I7 and I8.

Figure 7 shows the KAM maps of the initial and polished surfaces in the three areas. Since the GND densities are
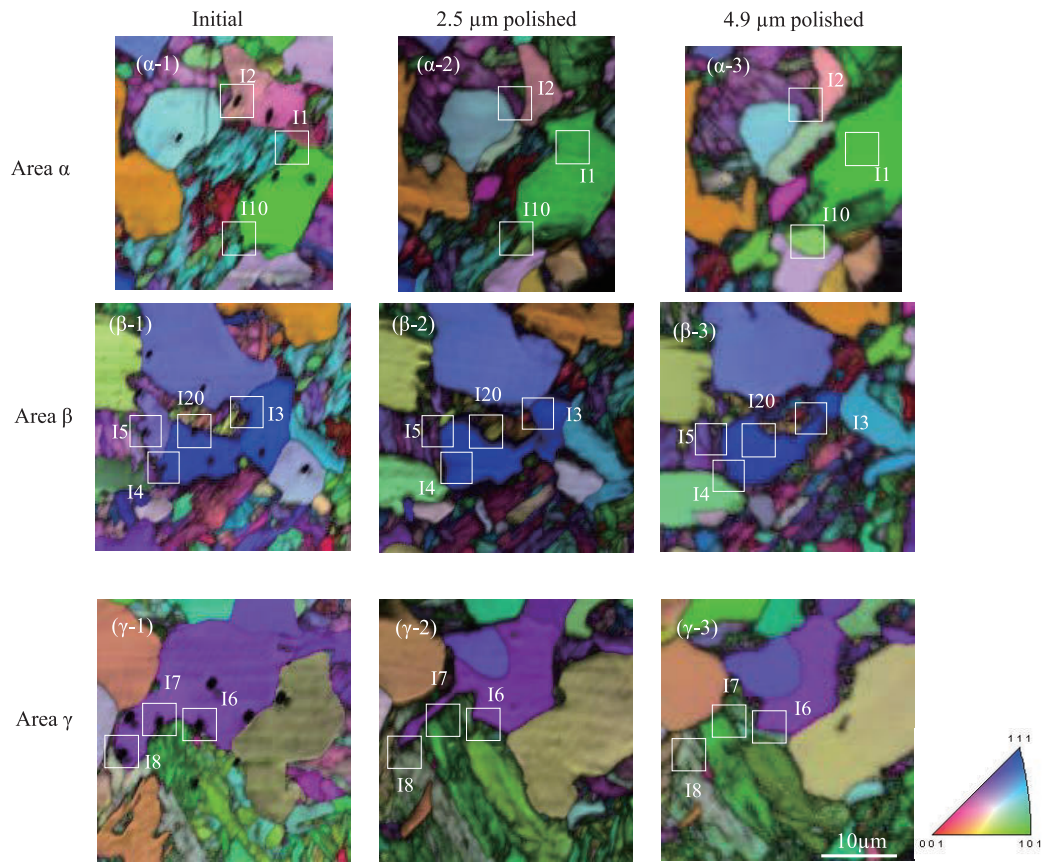
Fig. 6. Image quality and inverse pole figure (IQ+IPF maps) of the microstructures around the nanoindentations before and after polish.
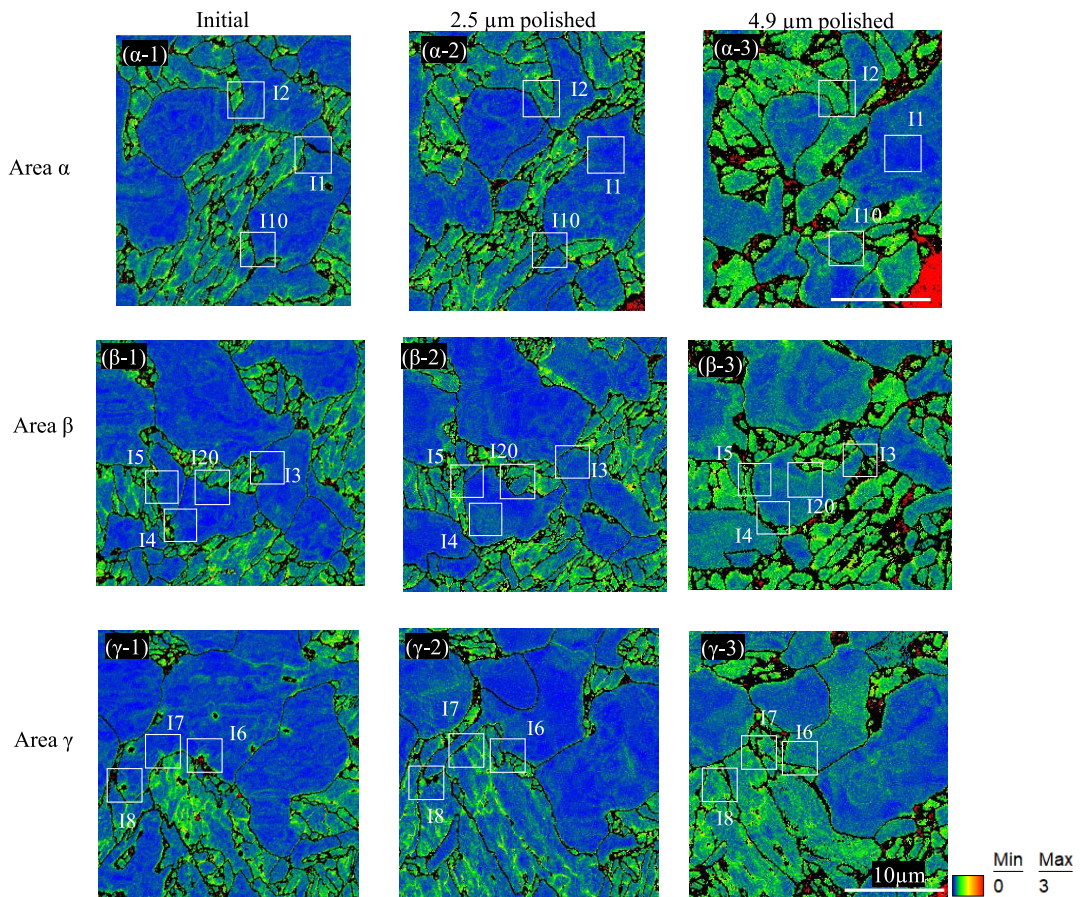

Fig. 7. Kernel Average Misorientation (KAM) maps of the microstructures around the nanoindentations before and after polish. The black lines indicate grain boundaries.

calculated from the KAM values,[20] the KAM map provides the qualitative tendencies of GND. As the first evident trend, Fig. 7 suggests that the KAM values were high in the martensite and low in the ferrite regions. In more detail, the intermediate KAM values were found to be distributed on the ferrite close to the ferrite–martensite interface in some locations. The whole ferrite region surrounding the martensite island did not exhibit much higher KAM values than those shown on the ferrite plane (the ferrite sufficiently distant from the martensite). Instead, the KAM values were high at some spotty distributed locations on the ferrite, especially on the ferrite–ferrite grain boundaries. Generally, KAM values at the grain boundaries are high because KAM is defined as the average of the crystal orientation differences of neighboring measurement points. Nevertheless, the above-mentioned ferrite locations with irregularly high KAM values were unaffected by this unavoidable natural trend because relative to the area of such high KAM ferrite locations, because the step size for the EBSD analysis (0.04 μm) was sufficiently small.

3.3. Nano-hardness

Figure 8 shows the nano-hardness measurement results for areas α and β with a force of 1 000 μN. The nano-hardness measurements in area α exponentially decreased with an increase in the distance from the ferrite–martensite interface. Scattered nano-hardness measurements, which were defined as deviated values from the exponential decrease rule, were few in this area. Nonetheless, some scattered nano-hardness values were measured in area β. Notably, the nano-hardness of indents I4 and I5 deviated to the higher side of the exponential decrease curve of the nano-hardness versus distance. In particular, the hardness
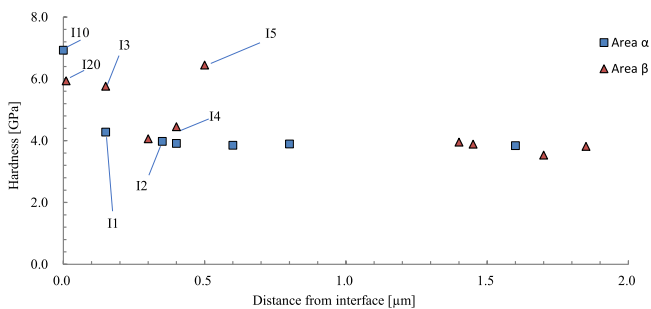
at indent I5 was equal to the hardness immediately above the ferrite–martensite interface (where the distance is zero). Compared with the nano-hardness distribution in area α, that at indent I3 was also regarded as the scattered value. Although the distance of indent I3 in area β was similar to that of indent I1 in area α, the hardness at indent I3 was much higher than that at indent I1. For the overall measurements in areas α and β, the nano-hardness values were converged to approximately 3.6 GPa at a distance of 0.3 μm, whereas the scattered nano-hardness at indents I4 and I5 were excluded from this convergence analysis. It should be noted that the distance of 0.3 μm was equivalent to the indent size (diameter), as shown in Section 3.1.

For the nano-hardness in area γ, **Fig. 9** shows the measurements with respect to the distance from the interface. Evidently, the nano-hardness measurements at indents I6, I7, and I8 presented scattering behaviors. Looking at indents I6 and I7, the nano-hardness at indent I6 was lower than that at indent I7, but indent I6 was closer to the ferrite–martensite interface. For indent I8, the nano-hardness was lower than that of the ferrite phase (nano-hardness at a distance of 1.0 μm or more). The convergence of nano-hardness was established at a distance of approximately 0.6 μm; this distance was larger than that in areas α and β. Similar to the cases in areas α and β, the convergence distance in area γ approximately corresponds with the indent size (diameter) shown in Section 3.1.

4. Discussion

The results in Section 3.3 refuted the assumption of the preliminary hardening site surrounding the martensite islands reported for fine-grained DP steels. The nano-hardness measurements converged to the ferrite values at a distance exceeding the indent size (diameter), whereby some scattered nano-hardness values were measured. This convergence is consistent with the deformation areas according to nanoindentations. Assuming that the indent areas observed in the SEM images and EBSD map corresponded with the deformed areas, we could establish that only the ferrite phase deformed in the nanoindentation measurements when the indent areas did not include the martensite part. Therefore, the nano-hardness measurements are converged at a distance exceeding the indent size; such a nano-hardness behavior is consistent with the results obtained from FE simulations.[17] If the preliminary hardening site was uniformly surrounding the ferrite–martensite interfaces, this convergence distance would never correspond with the indent size. However, we should note that the aforementioned nano-hardness convergence is the average trend in the measurements; the scattered nano-hardness measurements were not negligible. As mentioned in Section 1, the scattered nano-hardness measurement was possibly caused by the spotty distribution of the GND densities. To find such local hardening (softening) sites around the interface, the scattering caused by the hidden interface shape should be denoised. Based on these findings, the scattered nano-hardness measurements are factorized in the following sections. The factorization was discussed based on the assumption that the neighboring indents had minimal influence on the nano-hardness measurements. This assumption was valid considering the results of the IQ

Fig. 8. Nano-hardness of ferrite near the ferrite-martensite interface in Area α and Area β measured with 1 000 μN force. (Online version in color.)
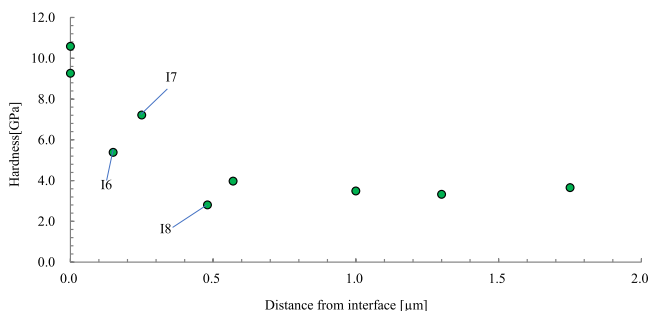

Fig. 9. Nano-hardness of ferrite near the ferrite-martensite interface in Area γ measured with 2 000 μN force. (Online version in color.)

maps. In Fig. 6, the indent areas with low IQ values are not overlapped. In addition, the following discussion is based on the interpolated interface shape under the assumption that the monotonic shape changes with an increase in the depth from the indented surface, wherein the sheared-off layer with a thickness of 2.5 μm exceeds the indentation depth.

Firstly, the scattered nano-hardness in area α is discussed. As mentioned in Section 3.3, there was a little scattering found in area α. However, focusing on indent I1, the distance between the indented center and ferrite–martensite interface increased at the two polished surfaces, as shown in (α-2) and (α-3) in Figs. 5 and 6. The increased ferrite fraction observed in indent I1 presumably caused a deviation (on the lower side) in the nano-hardness evaluation. Compared with the measurement at indent I3 in area β, the value at indent I1 was much lower despite the equal distance from the ferrite–martensite interfaces. It should also be noted that the nano-hardness at indent I3 deviated to the higher sides mentioned in the following paragraph. In contrast to the measurement at indent I1, hidden martensite phases were present under the ferrite surface at indent I2, as seen in Fig. 6(α-2). Although this hidden martensite was expected to increase the nano-hardness, the nano-hardness at indent I2 was almost equal to that of the ferrite. We could not determine the reason why the nano-hardness presented such a low nano-hardness side deviation at indent I2. However, two hypotheses were formulated, as follows: The hidden interface shape close to indent I2 was significantly different from that at the 2.5 μm-polished surface. The local fraction of the ferritic phase increased the depth from the indented surface. Additionally, the scattered carbon densities possibly generated local softening sites on the martensite. Notably, the carbon densities on the martensite were reported in DP steels, particularly around the interfaces.[21]

Secondly, the nano-hardness scattering in area β is discussed. For indent I3, it is evident from Fig. 6(β-2) that the interface shape changed subtly before and after polishing. Thus, the nano-hardness should not be scattered. However, the nano-hardness measurement at indent I3 deviated to the higher side. Notably, the nano-hardness at indent I3 was similar to that just above the interface (at indent I20). A comparison with the nano-hardness curve in area α also showed this deviation for indent I3. The nano-hardness at indent I3 deviated from the exponential decrease rule with an increase in the distance.[17] The nano-hardness at indent I3 presented almost linear-interpolated values at distances of 0 μm (at indent I10) and 0.4 μm (at indent I2) from the interface. The high KAM values may have caused this higher side deviation of the nano-hardness measurement. From Fig. 7 (β-1), the KAM values were high around indent I3, and therefore, the GND density was also high. Although this high GND density may have been caused by the nanoindentation, it may be expressed as a high nano-hardness at indent I3. A higher fraction of martensitic phase was observed on indent I20 than on I10 above the interface (indents I10 and I20 are present in areas α and β, respectively) at the polished surface (Figs. 6(α-1) and 6(β-1)). Nevertheless, the nano-hardness measurement at indent I20 was lower than that at indent I1 by approximately 1.0 GPa. This same tendency is observed with indent I2. The two aforementioned hypotheses projected this nano-hardness deviation to the

lower side. For indent I5, the nano-hardness measurement deviated to the higher side, wherein the evaluation exceeded the value at indent I20 (zero distance from the interface). The reason for this deviation is evident. From Fig. 6(β-2), the martensite was hidden under the ferrite surface at indent I5. Conversely, indent I4 revealed a ferrite area enlargement at the 2.5 μm-polished surface, whereas the nano-hardness was slightly higher than the convergence value. The high KAM values (GND densities) probably caused this higher side deviation at indent I4. The high KAM value region was established around indent I4, as shown in Fig. 7(β-1), similar to the case of indent I3.

Finally, the nano-hardness scattering in area γ was discussed. As apparent in Figs. 6(γ-1), 6(γ-2), the interface shape changed little around indent I6 in area γ after the polishing. Therefore, the hidden microstructure did not influence the nano-hardness measurement at indent I6. The nano-hardness at indent I6 exponentially decreased from the value just above the interface. The nano-hardness at indent I7 was more deviated to the higher side than at indent I6. The presence of martensite under the initial ferrite surface caused this deviation, as shown in Fig. 6(γ-2). For indent I8, the nano-hardness was evidently deviated to the lower side, despite the presence of the hidden martensite shown in Fig. 6(γ-2). Compared with the ferrite nano-hardness, the value at indent I8 was lower. The lower side nano-hardness deviation in both the ferrite and martensite probably caused this behavior around indent I8. Based on the indentation force, no remarkable effects were found except for the nano-hardness just above the interfaces from the comparison between the measurements with the indentation forces of 1 000 μN (areas α and β) and 2 000 μN (area γ).

Summarily, the preliminary hardening sites along the ferrite–martensite interface that were reported for fine-grained DP steel were not found in this study. The measured KAM (GND) map supported this analysis. However, some scattered nano-hardness measurements implied the existence of spotty hardening sites on the ferrite close to the interface, whereby most of the scattering was caused by the hidden microstructure under the indented surface. The heterogeneous distribution of high GND densities possibly caused these spotty hardening sites. More interestingly, however, some nano-hardness measurements indicated the existence of local softened sites of ferrite close to the interface, which were adducible to the spatial scattering of the carbon density. The denoising of the hidden microstructural effect from the nano-hardness scattering successfully revealed the existence of such softening sites. The authors have presented this discussion to clarify the effect of local hardening/softening sites on the mechanical properties of this material that could be important for future applications.

5. Summary

In this study, the nano-hardness distribution near the ferrite–martensite interface was investigated in the conventional coarse-grained DP steel. We focused on the scattering factors in the nano-hardness measurements. The effect of hidden microstructures under the indented surface was denoised from the scattering of nano-hardness measurements to classify the scattering caused by the preliminary

hardening sites around the previously reported interface. The two-stage sequential polishing and SEM/EBSD analyses were conducted to investigate the interface shapes hidden under the indented surface. The conclusions are as follows:

(1) Excluding the scattering values, the nano-hardness measurements converged to the ferrite values at the distance of the indent diameter from the ferrite–martensite interface.

(2) Most of the higher side nano-hardness deviations were caused by the hidden martensite under the indented surface. In some deviated nano-hardness measurements, hidden martensite was not found, but the KAM values were high around the indent site on the ferrite. The spotty hardening sites were deduced from these observations.

(3) Most of the lower side nano-hardness deviations were caused by the increase in the ferrite area under the indented surface. However, some notable exceptions were found: the hidden martensite cases resulted in the lower side nano-hardness deviations. In this study, the detailed mechanism of such inconsistent scattering with the hidden microstructure could not be elucidated. However, one of the plausible hypotheses drawn from this work is the existence of local softening sites on both the ferrite and martensite.

Acknowledgments

REFERENCES

1) M. Takahashi: *Nippon Steel Tech. Rep.*, (2003), No. 88, 2, https://www.nipponsteel.com/en/tech/report/nsc/pdf/n8802.pdf, (accessed 2020-11-26).

2) J. Lee, S. Lee and B. C. De Cooman: *Mater. Sci. Eng. A*, **536** (2012), 231. https://doi.org/10.1016/j.msea.2012.01.003

3) A. S. Khan, M. Baig, S.-H. Choi, H.-S. Yang and X. Sun: *Int. J. Plast.*, **30–31** (2012), 1. https://doi.org/10.1016/j.ijplas.2011.08.004

4) K. Hasegawa, Y. Toji, H. Minami, H. Ikeda, T. Morikawa and K. Higashida: *Tetsu-to-Hagané*, **98** (2012), 320 (in Japanese). https://doi.org/10.2355/tetsutohagane.98.320

5) P.-H. Chang and A. G. Preban: *Acta Metall.*, **33** (1985), 897. https://doi.org/10.1016/0001-6160(85)90114-2

6) M. Kurita, K. Toyama, S. Nomura and K. Kunishige: *Tetsu-to-Hagané*, **81** (1995), 1091 (in Japanese). https://doi.org/10.2355/tetsutohagane1955.81.11_1091

7) H. Lyu, A. Ruimi and H. M. Zbib: *Int. J. Plast.*, **72** (2015), 44. https://doi.org/10.1016/j.ijplas.2015.05.005

8) S. Sun and M. Pugh: *Mater. Sci. Eng. A*, **335** (2002), 298. https://doi.org/10.1016/S0921-5093(01)01942-6

9) T. Matsuno, T. Yoshioka, I. Watanabe and L. Alves: *Int. J. Mech. Sci.*, **163** (2019), 105133. https://doi.org/10.1016/j.ijmecsci.2019.105133

10) D. Das and P. P. Chattopadhyay: *J. Mater. Sci.*, **44** (2009), 2957. https://doi.org/10.1007/s10853-009-3392-0

11) A. Fillafer, E. Werner and C. Krempaszky: *Mater. Sci. Eng. A*, **708** (2017), 556. https://doi.org/10.1016/j.msea.2017.10.005

12) J. Kadkhodapour, S. Schmauder, D. Raabe, S. Ziaei-Rad, U. Weber and M. Calcagnotto: *Acta Mater.*, **59** (2011), 4387. https://doi.org/10.1016/j.actamat.2011.03.062

13) A. Ramazani, K. Mukherjee, A. Schwedt, P. Goravanchi, U. Prahl and W. Bleck: *Int. J. Plast.*, **43** (2013), 128. https://doi.org/10.1016/j.ijplas.2012.11.003

14) G. Avramovic-Cingara, Y. Ososkov, M. K. Jain and D. S. Wilkinson: *Mater. Sci. Eng. A*, **516** (2009), 7. https://doi.org/10.1016/j.msea.2009.03.055

15) T. Matsuno, D. Maeda, H. Shutoh, A. Uenishi and M. Suehiro: *ISIJ Int.*, **54** (2014), 938. https://doi.org/10.2355/isijinternational.54.938

16) T. Matsuno, C. Teodosiu, D. Maeda and A. Uenishi: *Int. J. Plast.*, **74** (2015), 17. https://doi.org/10.1016/j.ijplas.2015.06.004

17) T. Matsuno, R. Ando, N. Yamashita, H. Yokota, K. Goto and I. Watanabe: *Int. J. Mech. Sci.*, **180** (2020), 105663. https://doi.org/10.1016/j.ijmecsci.2020.105663

18) A. Ebrahimian and S. S. Ghasemi Banadkouki: *J. Alloy. Compd.*, **708** (2017), 43. https://doi.org/10.1016/j.jallcom.2017.02.287

19) F. S. LePera: *JOM*, **32** (1980), 38.

20) D. P. Field, P. B. Trivedi, S. I. Wright and M. Kumar: *Ultramicroscopy*, **103** (2005), 33. https://doi.org/10.1016/j.ultramic.2004.11.016

21) C. P. Scott, B. Shalchi Amirkhiz, I. Pushkareva, F. Fazeli, S. Y. P. Allain and H. Azizi: *Acta Mater.*, **159** (2018), 112. https://doi.org/10.1016/j.actamat.2018.08.010